SPECT Quantification: A Simplified Method of Attenuation and Scatter Correction for Cardiac Imaging

James R. Galt, S. James Cullom and Ernest V. Garcia

Department of Radiology, Emory University School of Medicine, Atlanta, Georgia and Veterans Affairs Medical Center, Atlanta, Georgia

The quantitative and visual interpretation of SPECT myocardial perfusion images is limited by physical factors such as photon attenuation, Compton scatter, and finite resolution effects. A method of attenuation correction is described for use in nonhomogeneous media and applied to cardiac SPECT imaging. This method, termed multiplicative variable attenuation compensation (MVAC), uses tissue contours determined from segmentation of a transmission scan to assign a priori determined attenuation coefficients to different tissue regions of the transaxial images. An attenuation correction map is then constructed using a technique inspired by Chang's method that includes regionally dependent attenuation within the chest cavity and is applied after reconstruction by filtered backprojection. Scatter correction using the subtraction of a simultaneously acquired scatter window image enables the use of narrow beam attenuation coefficients. Experimental measurements to evaluate these methods were conducted for ^{201}Tl and ^{99m}Tc SPECT using a homomorphic cardiac phantom. Finite resolution effects were included in the evaluation of results by computer simulation of the three-dimensional activity distribution. The correction methodology was shown to substantially improve both relative and absolute quantification of uniform and nonuniform regions of activity in the phantom's myocardial wall.

J Nucl Med 1992; 33:2232–2237

The interpretation and quantification of single-photon emission computed tomographic (SPECT) images are hampered by the physical factors of photon attenuation, Compton scatter, and finite resolution effects. Compensation for these effects is particularly difficult in cardiac perfusion imaging since the heart is surrounded by other organs of varying density. The methods of attenuation correction commonly distributed with commercial SPECT systems (*1,2*) assume uniform attenuation within the body and prove ineffective for cardiac imaging. This report describes a method of attenuation correction for use in nonhomogeneous media that may be applied to cardiac SPECT. The attenuation correction method, termed multiplicative variable attenuation compensation (MVAC), uses tissue contours determined from segmentation of a transmission scan to assign a priori determined attenuation coefficients to different tissue regions of the transaxial images.

Information about the anatomy of the patient required for attenuation correction of SPECT images in nonhomogeneous media is not readily available from a standard emission scan. Several methods that use a transmission scan to reconstruct a map of attenuation coefficients within the subject have been developed and studied (*3–7*). However, these methods are bound to the inaccuracies of the determination of attenuation coefficients due to the significant Poisson noise, scattering of photons and scaling during the reconstruction process. The use of simultaneous emission and transmission acquisitions with the gamma camera requires the use of two radionuclides with sufficiently different energy to prevent the corruption of one image by photons from the other radionuclide. In this situation, to successfully correct for attenuation, the relationship between the absorption properties for the two different energies must be known. Furthermore, transmission scans of sufficient statistical accuracy to calculate the attenuation values directly imply a significant radiation dose to the patient and a longer study time.

These difficulties in determining an accurate map of the attenuation coefficients may be reduced by using the transmission transaxial slices to determine the boundaries between areas of different density. A method first suggested by Budinger (*8*) would assign a priori determined attenuation coefficients to the areas identified in the transaxial images. With this approach, the required statistical accuracy is reduced and a relatively short transmission scan may be used, reducing the time the patient must remain on the imaging table as well as the patient's radiation dose. This approach has recently been investigated for PET by Xu (*9*), who was able to reduce the transmission scan time from 30 to 10 min while maintaining the quantitative capability with ^{13}N-ammonia.

Received Jan. 2, 1992; revision accepted Jun. 11, 1992.

For reprints contact: James R. Galt, PhD, Department of Radiology, Emory University School of Medicine, 1364 Clifton Rd, N.E., Atlanta, GA 30322.

Quantitative imaging also requires correction for the effects of Compton scatter. In this study, a scatter correction methodology is used which subtracts a fraction of a simultaneously acquired scatter image from the photopeak image (containing scatter) is suggested by Jaszczak (*10*).

In the experiments described here, scatter correction is applied first. The MVAC method is then applied to the scatter corrected transaxial images and evaluated for quantitative cardiac imaging in phantoms with ^{201}Tl and ^{99m}Tc. Evaluation consists of quantitative comparison of maximal count circumferential profiles (MCCPs) extracted from the phantom images with the count distribution expected in the absence of attenuation and scatter.

METHODS

Scatter Correction Methodology

Implementation of the scatter correction methodology requires that planar images be acquired simultaneously over the photopeak and a scatter region of the spectrum. The primary (or photopeak) window produces the image to be used clinically and primarily contains photons of energies near the photopeak. The secondary (or scatter) window is placed over a lower energy region of the spectrum and therefore contains a significantly higher percentage of scatter photons than the primary window. Once the data have been acquired and the transaxial images reconstructed, the scatter correction is applied as follows:

$$f_c(x, y) = f_p(x, y) - kf_s(x, y),$$

where $f_s(x, y)$ is the scatter window image, $f_p(x, y)$ is the primary window image, k is the scatter window fraction (SWF) which must be determined a priori, and $f_c(x, y)$ is the corrected photopeak image.

The use of a constant scatter window fraction for all pixels assumes a linear relationship between the counts in the scatter window and the scattered counts in the photopeak window. The validity of this assumption has not been addressed directly in this work. However, Koral has recently investigated the dependence of quantitative accuracy with ^{99m}Tc SPECT on the value of the scatter window fraction (*11*). He found that the use of a constant scatter window fraction was a good first approximation for quantitative accuracy for different source sizes and position within a homogeneous attenuating media.

The photopeak and scatter windows used in the experiments described here for ^{201}Tl were 72 keV, 20% and 60 keV, 15% respectively and for ^{99m}Tc were 140 keV, 20% and 106 keV, 32% respectively. The photopeak windows for each isotope are those commonly used in the clinic. The ^{99m}Tc scatter window is broad (to maximize counts) and covers the Compton plateau. The ^{201}Tl scatter window covers the energy range below the photopeak window allowed by the scintillation camera. Earlier experiments with ^{99m}Tc line sources (*12*) gave results consistent with those reported by Jaszczak (*10*) and indicated a ^{99m}Tc scatter window fraction of 0.5. The geometry of the cardiac phantom used here is much more complex and therefore different scatter window fractions were evaluated for both isotopes.

Attenuation Correction Methodology

A transmission scan was acquired for the phantom measurements with 30 mCi of ^{99m}Tc in a collimated fillable flood source mounted opposite and parallel to the camera surface. Acquisition parameters included: a 140 keV, 20% energy window, 64 × 64 matrix (6 mm pixels), 64 views at 40 sec per view, 360° circular orbit, and low-energy, all-purpose (LEAP) collimation. The transmission scan was acquired prior to the emission scan without moving the phantom or table position to avoid alignment problems. The transmission transaxial slices were reconstructed using filtered backprojection after decay and flood correction. These images were then segmented into soft-tissue and lung regions by thresholding.

Attenuation coefficients were determined experimentally by applying linear regression to the measured count rate as various thicknesses of water (soft tissue) and Styrofoam (lung) were placed between a collimated photon source and a scintillation camera (*12*). Coefficients assigned for ^{201}Tl were 0.176 cm^{-1} and 0.018 cm^{-1} for water and Styrofoam, respectively. Coefficients assigned for ^{99m}Tc were 0.154 cm^{-1} and 0.015 cm^{-1}. It was not possible to differentiate between water and other dense material in the transmission images. The imaging table was visible in the transmission images and was assigned the same value as the lung. All pixels outside of the segmented body boundary and table and in the central lung region were assigned a value of zero for air.

The correction map derived from the attenuation coefficient map is similar in formulation to the first order (no iterations) correction described by Chang (*2*). The attenuation at any given pixel location within the transaxial image is approximated by the average attenuation experienced by photons originating in that voxel for all measured projections. A significant departure from Chang's method as it is commonly applied is the incorporation of varying linear attenuation coefficients. The correction factors at each point are computed using the assigned attenuation coefficient values from the segmented transmission image with the equation:

$$C(x, y) = \left[\frac{1}{M}\sum_{i=1}^{M}\left(\prod_{j=1}^{N} e^{-\mu^{j(x,y,\theta_i,r_j)}l_j(x,y,\theta_i,r_j)}\right)\right]^{-1},$$

where the correction factor C for each point (x, y) in the transaxial image is the average of the attenuation factors for projections at M angles (θ_i) over 360° around the point. Each attenuation factor is the product of the attenuation due to each of the N voxels defined by the radial distance from the point (r_j) along the projection angle (μ_j is the attenuation coefficient for the jth voxel, l_j is the length of the projection through this voxel).

A simplified version of Sorenson's method of attenuation correction (*1*) which was commercially available was also used for comparison of our results. This version assumes uniform attenuation (effective attenuation coefficient value of 0.12 cm^{-1}) and that the activity is distributed uniformly within the medium.

Convolution Model

To evaluate the effects of finite resolution on quantification, a three-dimensional convolution was performed on a computer simulation of the phantom configurations. The point spread function (PSF) used in the model was a spherically symmetric Gaussian function with a half-width-at-half-maximum (HWHM) of 9 mm and 8 mm for ^{201}Tl and ^{99m}Tc respectively and was assumed to be invariant over the region of the distribution. The resulting image is that expected under ideal conditions in the absence of attenuation, scatter and noise (*13*). MCCPs from the simulated images were used as the baseline for evaluation of the correction methodology after calibration.

The assumptions made about the PSF in the simulation are

only valid if the experimental PSF varies only slightly in the area occupied by the heart. This approximation is supported by the use of 360° camera orbits and the fact that noise reducing filters were applied equally in all three dimensions. Application of the methods presented here to 180° orbits will require compensation for spatially varying resolution and will be addressed in the later report. Even with these assumptions attenuation and scatter will cause the shape of the PSF to vary, particularly near attenuation boundaries. These variations are largely corrected by the methods proposed here.

Phantom Experiments

The phantom used to evaluate the correction methodology is a Data Spectrum Cardiac Insert (model 7070) mounted in a Data Spectrum Elliptical Phantom (model 2230) (Fig. 1). Lung inserts, made of Styrofoam, and a spine insert, made of packed bone meal, were developed in-house. Fillable defect chambers, with different activity concentrations, were placed around the mid-ventricular circumference of the phantom in a ring configuration. This ring of defects was 2 cm in length along the long axis and placed in the center of the myocardial wall so that there were areas of normal myocardium both above and below the ring of defects. Three fillable defects were used, spanning 180°, 90°, and 45°, with tracer concentrations of 50%, 75%, and 25% of the normal wall concentration respectively. The remaining 45° was open to allow for even mixing of activity through the normal wall. This distribution of activity is shown in Figure 2 along with the image predicted by the convolution model for ^{99m}Tc (HWHM of 8 mm). The activity concentrations in the normal wall were 15 μCi/cc for ^{201}Tl and 16.5 μCi/cc for ^{99m}Tc with a normal myocardial wall volume of approximately 90 ml. Background activity in the ventricular chamber and phantom body was 5% of the normal myocardial wall concentration.

Sixty-four views were acquired using a 64 × 64 matrix over a 360° orbit, a LEAP collimator and a circular orbit which contoured the phantom as close as possible. The time per view was 40 sec for ^{201}Tl and 60 sec for ^{99m}Tc. The photopeak and scatter energy windows were as described above. Before transaxial reconstruction, both the photopeak and scatter window projections were filtered with a two-dimensional symmetric Hann filter with a cutoff frequency of 0.833 cycles/cm.

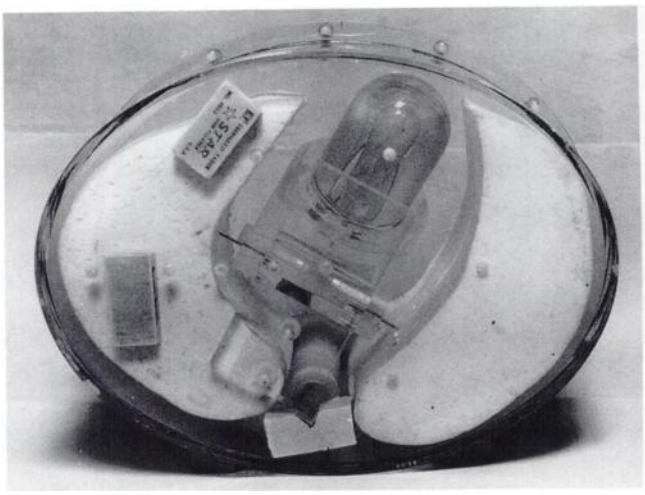

FIGURE 1. Phantom thorax. The Data Spectrum elliptical phantom is shown with the Data Spectrum cardiac insert. Lung inserts and a spine insert were developed in-house.

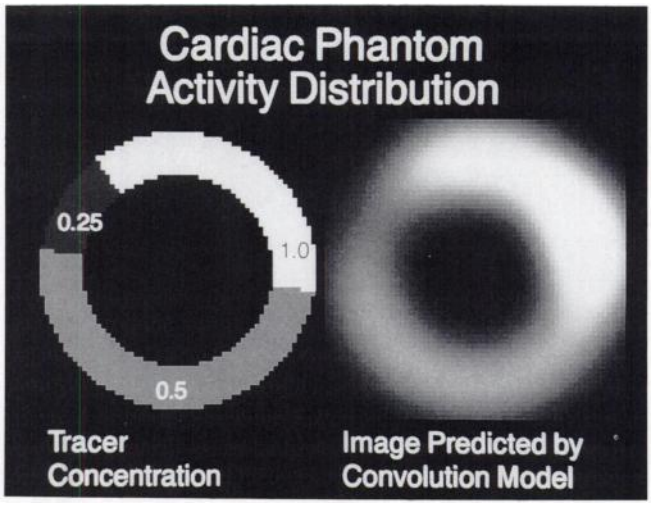

FIGURE 2. Distribution of activity in the cardiac phantom. The left panel shows the distribution of activity (achieved with three fillable chambers) used in the myocardial wall of the cardiac phantom. The 2-cm long chambers spanned 180°, 45° and 90° with tracer concentrations of 50%, 25% and 75% of the "normal" wall concentration, respectively. The right panel shows the short-axis image expected in the absence of attenuation and scatter (predicted by the convolution model).

RESULTS

The correction methodology is illustrated in Figure 3 for the ^{201}Tl phantom experiment. Panel A shows the transmission transaxial slice of the phantom thorax with a cardiac insert. The cardiac insert contained activity at the time of acquisition and can be seen in this image. Panel B

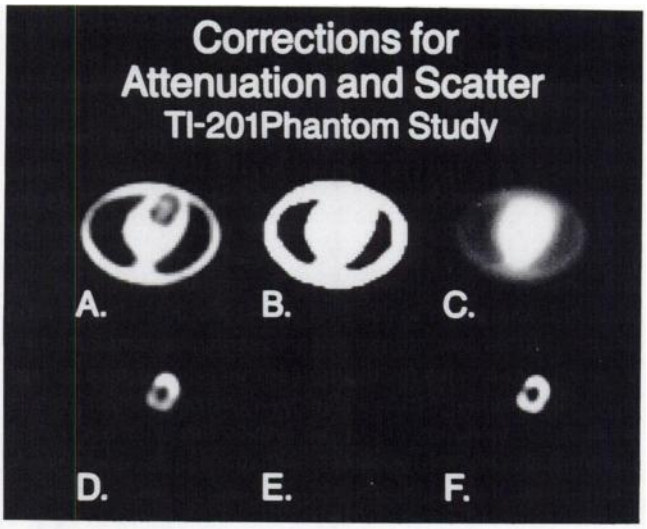

FIGURE 3. Thallium-201 phantom study, attenuation and scatter corrections. (A) Transmission transaxial slice of the phantom thorax. The cardiac insert contained activity when this image was made and is visible. (B) Map of assigned attenuation coefficients. (C) Attenuation correction map. (D) Corresponding photopeak emission transaxial slice through the phantom's myocardial wall chamber. (E) Scatter emission transaxial slice (scaled to show relationship to D). (F) Scatter and attenuation corrected emission transaxial tomogram.

shows how regions have been defined and a priori determined attenuation coefficients assigned. Panel C shows the attenuation correction map constructed from Panel B. Panels D and E show transaxial slices through the cardiac insert acquired with the photopeak and scatter windows, respectively. These images have been scaled to show the relative magnitude of counts in the two windows. The image in Panel F shows the same transaxial slice with scatter and attenuation correction applied. Important items to note in the corrected image are the increased uniformity of the apical and basal regions of the phantom (which had the same ^{201}Tl concentration), the increased contrast of the defect in the septal wall, and the increased contrast of the ventricular chamber.

Relative Evaluation of the Corrections

Three short-axis slices of the phantom were chosen to evaluate the correction methodology on a relative scale: (1) a uniform basal slice, (2) a nonuniform slice through the center of the ring of defects, and (3) a uniform apical slice. These slices were extracted from the experimental images and simulated using the convolution simulation. Maximal count profiles through these slices were then normalized to the mean of the two uniform profiles to give a basis for comparison.

Figure 4 shows relative MCCPs for ^{201}Tl obtained for the ring of defects and normalized to the mean of the normal apical and basal profiles (uniform slices above and below the ring of defects). The simulation curve gives the response expected from the activity distribution with the system resolution (no attenuation or scatter) and forms the gold standard for our measurements (Fig. 4A). The defect with the lowest concentration can not be discerned in the raw count (uncorrected profile). Attenuation correction alone (SWF = 0.0) overestimates the true count values because the added counts due to scatter are neglected. Application of attenuation correction after scatter subtraction (Fig. 4B) clearly improves the correlation of corrected and predicted values over the range of defects. The normalized mean square error (NMSE) between the experimental and simulated profiles indicated best results with a scatter window fraction of 1.5.

The corresponding data for the ^{99m}Tc experiment are shown in Figure 5. The best correlation in MCCPs of measured and predicted counts for the ring of defects was obtained with a scatter window fraction of 0.5. These improvements are consistent with the results obtained for ^{201}Tl. As the figure shows, the commercially available method overestimated the activity in the ring of defects and did not substantially improve contrast in the area of least activity.

Absolute Evaluation of the Corrections

Absolute evaluation of the corrections requires an external calibration. This calibration was accomplished by tomographically imaging a 90° (5.5 ml) fillable chamber both in air and mounted in the lateral wall near the base of the filled cardiac phantom. An attenuation factor was

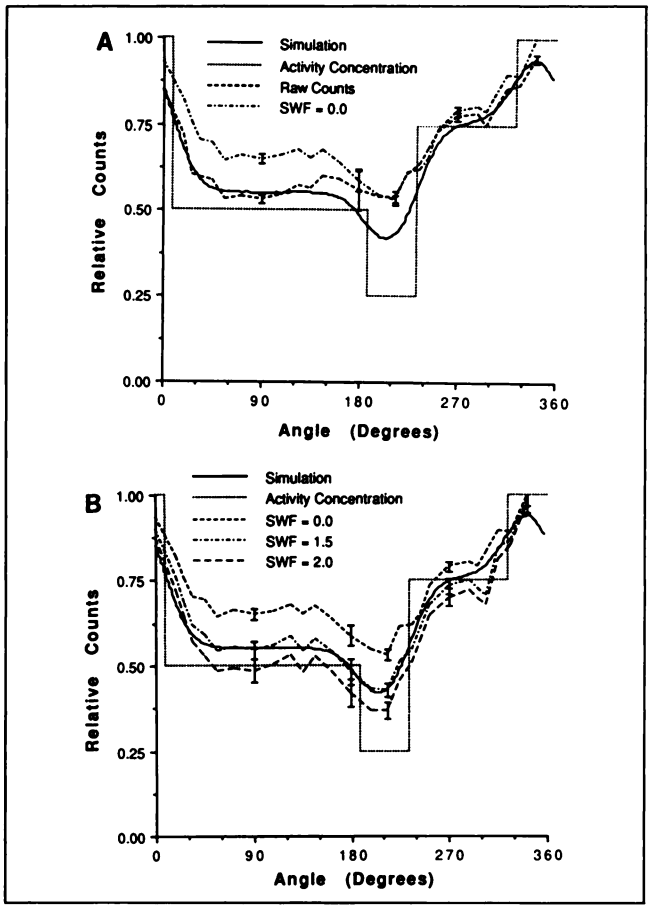

FIGURE 4. Thallium-201 cardiac phantom, relative count MCCPs. Maximal count circumferential profiles through the ring of defects normalized to the mean of two uniform slices (one above and one below the defects). Error bars represent statistical noise (estimated with SPECT simulation as two standard deviations). Error bars at 180° show rms deviation from uniformity of a uniform slice processed in the same manner during a separate experiment and thus represent the effects of all sources of error. (A) This plot shows the raw (uncorrected) counts and attenuation correction alone. (B) Similar to (A) but with scatter correction using different scatter window fractions (SWF). The best match was found with a scatter window fraction of 1.5.

derived as the ratio of counts extracted from the chamber mounted in the phantom (corrected for scatter) and counts extracted from the chamber in air (corrected for self attenuation). From this attenuation factor and the counts in the lateral wall of a basal slice of the phantom, a factor was found to scale the profiles predicted by the convolution model for comparison to absolute counts.

Evaluation of the corrected image profiles in terms of absolute counts compared the NMSEs between the counts from the experimental profiles and the scaled results of the simulation model. Best results were found with scatter window fractions of 2.0 and 1.0 for ^{201}Tl and ^{99m}Tc respectively.

Quantitative Evaluation of the Corrections

The results of the relative and absolute evaluation of the corrections are summarized in Table 1 for two uniform

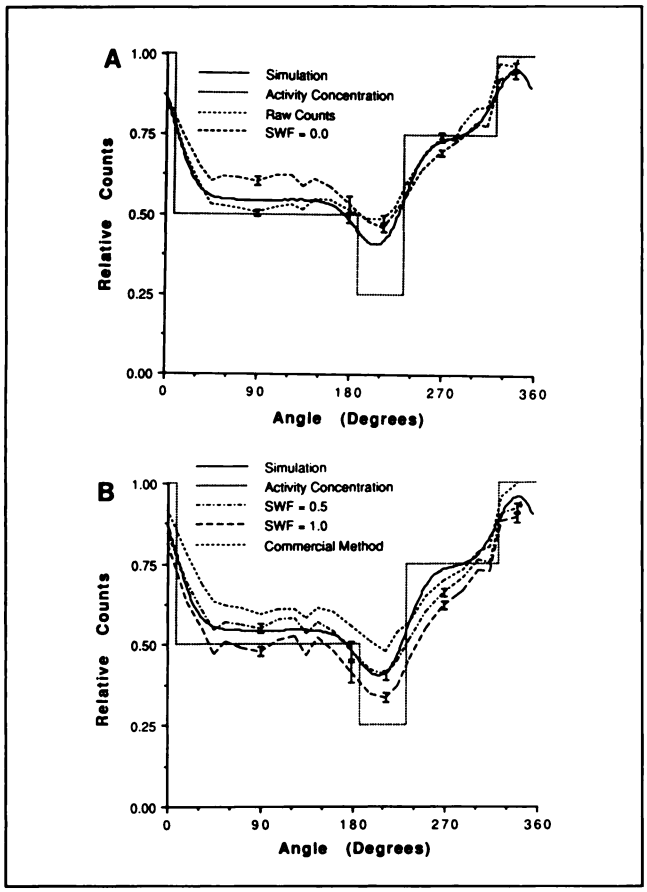

FIGURE 5. Technetium-99m cardiac phantom, relative count MCCPs. Maximal count circumferential profiles through the ring of defects normalized to the mean of two uniform slices. Error bars represent statistical noise (estimated with SPECT simulation as two standard deviations). Error bars at 180° show rms deviation from uniformity of a uniform slice processed in the same manner. (A) This plot shows the raw (uncorrected) counts and attenuation correction alone. (B) Similar to (A) but with scatter correction using different scatter window fractions (SWF). The best match was found with a scatter window fraction of 0.5. The commercial method is that supplied by the manufacturer and is a simplification of Sorenson's method.

short-axis slices (apical and basal) and through the ring of defects. Attenuation correction alone improved the uniformity of uniform slices, giving the greatest change in %NMSE. The addition of scatter correction degraded this uniformity to a small extent in the relative evaluation but when absolute counts were considered produced significantly improved results. The scatter window fraction that gave the best results for each radionuclide in the absolute evaluation was higher than that found for the relative evaluation and may reflect inaccuracies in the scaling of the results of the simulation to estimate absolute counts.

DISCUSSION

The limiting effects of Compton scatter, photon attenuation and finite resolution of the imaging system on myocardial perfusion imaging and quantification are well known. The nonhomogeneous distribution of attenuation within the thoracic cavity complicates the interpretation of these images and precludes the application of more simple methods of scatter and attenuation correction developed for homogeneous media. The latter methods generally require only knowledge of the external boundary of the object and the constant attenuation coefficient in the region. The method proposed here, which uses a transmission scan to provide information about the spatial variation in tissue attenuation coefficient and an interactive segmentation method for tissue boundary determination, avoids many of the problems of absolute determination of the attenuation coefficient by employing narrow beam values for correction of scatter subtracted images.

Scatter subtraction, which removes the broad scatter response superimposed on the photopeak PSF, can improve quantification by reducing the influence of scatter on surrounding structures. However, the reduced number of counts in the corrected image can result in increased image noise and a loss of uniformity over the normal myocardium. This method also results in a significant increase in contrast and therefore the possibility of im-

TABLE 1
Attenuation and Scatter Correction Evaluation

		Uniform apical		Uniform basal		Ring of defects	
Isotope	k	Relative %NMSE	Absolute %NMSE	Relative %NMSE	Absolute %NMSE	Relative %NMSE	Absolute %NMSE
^{201}Tl	Raw	7.31	36.9	4.41	52.6	0.61	45.4
	0.0	1.03	29.4	0.27	11.0	2.03	34.5
	1.0	1.10	12.5	0.30	3.0	0.60	9.0
	1.5	1.16	7.1	0.33	1.0	0.25	2.5
	2.0	1.26	2.2	0.39	0.1	0.71	0.5
^{99m}Tc	Raw	4.00	29.2	2.29	44.6	0.30	36.3
	0.0	0.63	25.9	0.10	15.6	0.58	22.9
	0.5	0.69	16.5	0.12	9.1	0.28	9.3
	1.0	1.79	8.8	0.14	4.0	1.15	1.5
	Com	1.44	21.4	0.57	4.9	0.93	16.6

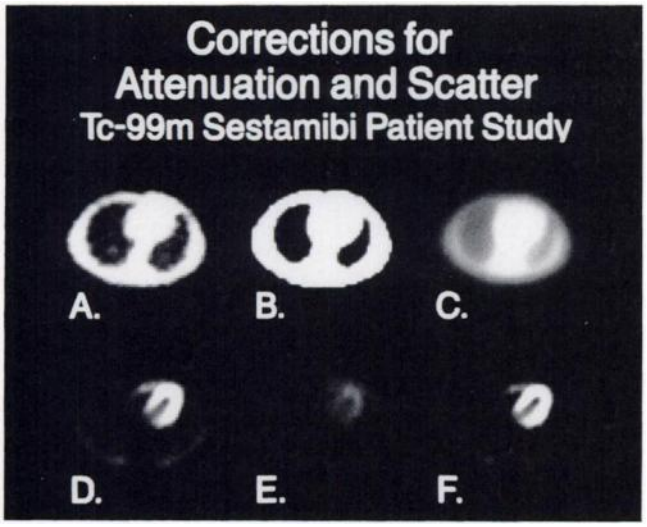

FIGURE 6. Technetium-99m-sestamibi patient study, attenuation and scatter corrections. (A) Transmission transaxial of the patient's chest. (B) Map of assigned attenuation coefficients. (C) Attenuation correction map. (D) Corresponding photopeak emission transaxial slice through the phantom's myocardial wall chamber. (E) Scatter emission transaxial slice (scaled to show relationship to D). (F) Scatter and attenuation corrected emission transaxial tomogram.

proved diagnostic value. By acquiring a second scatter window, the dependence of the scatter component of the photopeak image on surrounding activity is measured on a patient specific basis, reducing the number of assumptions required in the correction methodology. The dependence of scatter on the inhomogeneity of the media is also maintained. It should be noted that the scatter corrections applied here are independent of the MVAC method. Other promising methods of scatter correction such as that recently suggested by King (*14*) are not precluded.

We have evaluated the protocol described here clinically (Fig. 6) and found that it can be implemented with relatively minor modifications to a conventional single headed gamma camera gantry. The transmission image in Figure 6A was acquired in 11 min using a 30 mCi ^{99m}Tc collimated flood source. The most evident difficulty for using this methodology clinically is the required precautions for the registration of transmission and emission images.

This methodology is not restricted to the radionuclides (and photon energies) described here. In particular, the use of assigned rather than calculated attenuation coefficients circumvents the need for the transmission map to be adjusted for photon energy. The assignment of attenuation coefficients should reduce the statistical requirements of the study allowing for a quicker scan that saves the technologist time and reduces patient radiation exposure. Initial observations of ^{99m}Tc-sestamibi scatter images indicate that it may be possible to estimate the tissue contours without the use of a transmission scan.

CONCLUSIONS

The MVAC method applied to scatter subtracted transaxial images of the myocardium offers promise to provide a significant improvement in relative and absolute quantification for both ^{201}Tl and ^{99m}Tc myocardial perfusion imaging. This method can be implemented clinically with relatively simple modifications to conventional SPECT systems.

ACKNOWLEDGMENTS

This work was supported in part by the National Institutes of Health (NHLBI) under grants RO1 H141628 and RO1 H142052, and by the Veterans Administration Research Advisory Group (RAG) under grant 3022-0001. The authors thank David Rex Hamilton for his assistance with the phantom experiments and development of the software. We are grateful to the reviewers for their helpful comments and suggestions.

REFERENCES

1. Sorenson JA. Quantitative measurement of radioactivity in vivo by whole body counting. In: *Instrumentation in nuclear medicine, volume 2.* New York: Academic Press; 1974:311–348.
2. Chang LT. A method for attenuation correction in radionuclide computed tomography. *IEEE Trans Nucl Sci* 1978;25:638–643.
3. Bailey DL, Hutton BF, Walker PJ. Improved SPECT using simultaneous emission and transmission tomography. *J Nucl Med* 1987;28:844–851.
4. Manglos SH, Jaszczak RJ, Floyd CE, Hahn LJ, Greer KL, Coleman RE. Nonisotropic attenuation in SPECT: phantom tests of quantitative effects and compensation techniques. *J Nucl Med* 1987;28:1584–1591.
5. Ljunberg M, Strand SV. Attenuation and scatter correction in SPECT for sources in a nonhomogeneous object: a Monte Carlo study. *J Nucl Med* 1991;32:1278–1284.
6. Ljunberg M, Strand SV. Attenuation correction in SPECT based on transmission studies and Monte Carlo simulations of build up functions. *J Nucl Med* 1990;31:493–500.
7. Manglos SH, Bassano DA, Duxbury CE, Capone RB. Attenuation maps for SPECT determined using cone beam transmission computed tomography. *IEEE Trans Nucl Sci* 1990;37:600–608.
8. Budinger TF. Physical attributes of single-photon tomography. *J Nucl Med* 1980;21:579–592.
9. Xu EZ, Mullani NA, Gould KL, Anderson WA. A segmented attenuation correction for PET. *J Nucl Med* 1991;32:161–165.
10. Jaszczak RJ, Greer KL, Floyd CE, Harris CG, Coleman RE. Improved SPECT using compensation for scattered photons. *J Nucl Med* 1984;25:893–900.
11. Koral KF, Swailem FM, Buchbinder S, Clithorne NH, Rogers WL, Tsui BMW. SPECT dual-energy-window Compton correction: scatter multiplier required for quantification. *J Nucl Med* 1990;31:90–98.
12. Galt JR. Reconstruction of the absolute radionuclide distribution in a scattering medium from scintillation camera projections. PhD Dissertation, Emory University, Department of Physics, 1988; University Microfilm, Ann Arbor, MI.
13. Galt JR, Garcia EV, Robbins WL. Effects of myocardial wall thickness on SPECT quantification. *IEEE Trans Med Imaging* 1990;9:144–150.
14. King MA, Hademenos GJ, Glick SJ. A dual-photopeak window method for scatter correction. *J Nucl Med* 1992;33:605–612.